

A Small-Molecule Polycationic Crosslinker Boosts Alginate-Based Bioinks for Extrusion Bioprinting

Chongjian Gao, Lan Tang, Huawei Qu, Mingming Wu, Tian Zhou, Chunyi Wen, Pinpin Wang,* Nan Xu,* and Changshun Ruan*

The importance of bioink suitability for extrusion bioprinting tissue-like constructs cannot be overemphasized. Owing to their excellent accessibility, alginate (Alg)-based bioinks are widely used. However, the printability accuracy and post-printing stability of current Alg-based bioinks remain challenging, especially for large-size fabrication. Herein, an improvement strategy for pre-crosslinking and post-crosslinking of methacrylated Alg (AlgMA) bioinks in extrusion bioprinting is presented via introduction of methacrylated ϵ -polylysine (ϵ -PLMA) as a small-molecule polycationic crosslinker. Due to their electrostatic interaction and covalent bonding, ϵ -PLMA significantly reinforce the operability and prolong stability of AlgMA bioinks, in comparison with single-molecule Ca^{2+} or large-molecule methacrylated gelatin as pre-crosslinkers. Meanwhile, attributed to their regulation of a charged microenvironment (-345.25 to 121.55 mV) and hydrophilicity (26.64° to 52.00°), the cells in bioprinted AlgMA/PLMA constructs demonstrated improved viability and vitality. Therefore, such a strategy of introducing small-molecule cationic crosslinker ϵ -PLMA is a promising booster for improving Alg-based extrusion bioprinting, potential to extend its biomedical applications.

are commonly used due to their extracellular matrix (ECM) nature. Among them, alginate (Alg) is widely adopted for its low price and good mechanical properties. Fedorovich et al.^[2] encapsulated human bone marrow mesenchymal stem cells (hBMSCs) into sodium Alg bioink, and the viability of cells in the scaffolds constructed by extrusion bioprinting can reach more than 90%. To extend the usability, Jeon et al.^[3] used Alg microgel bioink to cryopreserve hBMSCs. After recovery, the activity and differentiation potential of hBMSCs were not affected by the freezing process, which overcomes the constraints that bioinks need to be prepared and used immediately, fulfilling biological long-term storage and on-demand use of bioink. Furthermore, Alg has been used as a frame-supporting component in blend bioink due to its printability. For instance, Zhang et al.^[4] used extrusion-based bioprinting to print sodium Alg-based bioink with human umbilical vein smooth muscle cells encapsulated in, and


constructed vasculature catheters through coaxial needles. However, the intrinsic bio-inertness of Alg-based bioinks inhibits cellular interactions in the printed scaffolds.^[5]

To overcome such drawbacks, two types of methods have been invented: modification with bioactive units^[6] and mixing with bioactive components.^[7] The most common approach to bioactive modification is RGD-grafting, which can not only trigger cell adhesion effectively but can also be used to address selectively certain cell lines and elicit specific cell responses.^[8] However, the

1. Introduction

Extrusion-based bioprinting is the most common approach used in biological additive manufacture, due to its advantages in large-scale fabrication and fast multi-material construction.^[1] Bioink is seen as a cell carrier and microenvironment for cells early after printing. Therefore, the two most essential characteristics of bioink are printability and biocompatibility. Natural hydrogels, from animal or plant sources (e.g., gelatin, silk, and alginate),

C. Gao, L. Tang, H. Qu, M. Wu, P. Wang, C. Ruan
Research Center for Human Tissue and Organs Degeneration
Institute of Biomedicine and Biotechnology
Shenzhen Institute of Advanced Technology
Chinese Academy of Sciences
Shenzhen 518055, China
E-mail: pp.wang@siat.ac.cn; cs.ruan@siat.ac.cn
C. Gao, C. Wen
Department of Biomedical Engineering
The Hong Kong Polytechnic University, Hung Hom
Hong Kong SAR, 999077 China

 The ORCID identification number(s) for the author(s) of this article can be found under <https://doi.org/10.1002/adfm.202310369>

DOI: 10.1002/adfm.202310369

L. Tang, C. Ruan
University of Chinese Academy of Sciences
Beijing 100049, China

T. Zhou
Research Center for Translational Medicine Research and Development
Institute of Biomedical and Health Engineering
Shenzhen Institute of Advanced Technology
Chinese Academy of Sciences
Shenzhen 518055, China

N. Xu, C. Ruan
Shenzhen People's Hospital (The Second Clinical Medical College, Jinan University; The First Affiliated Hospital
Southern University of Science and Technology)
Shenzhen 518020, China
E-mail: xu.nan@szhospital.com

modification of RGD peptides cannot change the alginate's rheological properties, which need a high concentration as bioink and the low Ca^{2+} -crosslink stability under long-period culture also restricts the development of Alg-based bioinks. As a result, many researchers try to blend bioactive pre-crosslinker with alginate; the most common one is methacrylated gelatin (GelMA), which has a large molecular weight with many bioactive sites. By forming interpenetrating double networks and electrostatic force^[9] between Alg and GelMA, the printability and mechanical properties have a significant improvement.^[10] However, the twisting of the two large polymer chains of GelMA and Alg extends the stirring time to avoid block in the nozzle and uneven cell distribution. Inevitably, long-period shear stress will reduce cell viability and vitality.^[11] As a result, the possibility of large-scale fabrication is limited by the production of large-volume bioink in one go.

Recently, polyelectrolyte-based pre-crosslinking materials have drawn much attention in three-dimension (3D) bio-manufacture area. By introducing cationic material (+) into anionic ink (-), the synergy within the polyelectrolyte ink can be tuned.^[12] By modulating cationic component and anionic component ratio, the charges within the polyelectrolyte ink can be tuned conveniently, resulting in a bio-friendly microenvironment. Indeed, many tissues and organs in the human body are electrically sensitive, such as the heart, blood vessels, nerves, skin, etc., so polyelectrolyte inks are very promising material in tissue engineering. For example, Wang et al.^[13] mixed oppositely charged gelatin nanospheres to form injectable and biodegradable colloidal gels. Based on this, our group also prepared polyelectrolyte ink with Alg and ϵ -polylysine (ϵ -PL).^[14] Under electrostatic interaction, they can be 3D-printed into large-scale self-supporting structures under ambient temperature conditions. Then, the surface charge of the scaffold was further strengthened with ϵ -PL coating, resulting in effectively promoted cell adhesion. However, cells cannot be encapsulated in this polyelectrolyte ink, due to its non-biocompatible post-crosslinking approach under 1-ethyl-3-(3-dimethylaminopropyl) carbodiimide (EDC) and N-hydroxysuccinimide (NHS) treatment.

Here, we report a photo-crosslinkable polyelectrolytic methacrylated Alg (AlgMA) based bioink with methacrylated ϵ -PL (ϵ -PLMA) introduced as a small-molecule polycationic crosslinker (Figure 1A). Photo-crosslinking provides spatiotemporal control over material reaction behavior, which can be leveraged to aid in fabricating 3D structures.^[15] Furthermore, light-based chemistries are typically very efficient while yielding minimal byproducts, an important consideration for manufacturing biocompatible constructs containing living cells.^[15] Thanks to the small molecular weight and excellent water-solubility of ϵ -PLMA, this bioink can be prepared with a short-time stirring of only 10 s. Furthermore, this bioink demonstrates a significant improvement on printability (Figure 1B,C), due to the electrostatic interaction between AlgMA and ϵ -PLMA. After printing, scaffolds can be photo-crosslinked for reinforcement, showing a greater shape stability than ionic crosslinked scaffolds. Subsequently, we screen the AlgMA to ϵ -PLMA ratio from the aspect of electrical properties, mechanical properties, rheological properties, and crucially, cytocompatibility, from which the optimal formulation emerged.

2. Results and Discussion

2.1. Preparation and Characterization of Polyelectrolyte Bioinks

According to a previous report,^[16] AlgMA (shown in Figure S1, Supporting Information) and ϵ -PLMA (shown in Figure S2, Supporting Information) were successfully synthesized. The photo-crosslinking behaviors of as-prepared AlgMA and ϵ -PLMA were shown in Figures S1A and S2A (Supporting Information), respectively. The methacrylation of Alg and ϵ -PL were confirmed with a degree of substitution (DS) of $28.17 \pm 0.61\%$ and $30.65 \pm 1.39\%$, respectively (Equations S1 and S2, Figure S1B–E, S2B–D, Supporting Information). The number average molecular weight (M_n) of AlgMA and ϵ -PLMA is 273 and 0.8 kDa, respectively (Equation S3, Figure S1F, and S2E, Supporting Information). It was reported that 8% (w/v) Alg bioink was used for printing large-scale structures.^[17] To figure out a suitable printing window for blending AlgMA/PLMA bioink,^[18] a series of ratio and solid contents were evaluated (Figure S3, Supporting Information), suggesting that at least 8% (w/v) of AlgMA is needed for printing and the ratio of AlgMA to ϵ -PLMA should be no larger than 1:2 (Figure S3, Supporting Information). Therefore, in further investigation, we prepared a series of AlgMA/PLMA polyelectrolyte bioinks by fixing AlgMA content to 8% (w/v) and increasing ϵ -PLMA content from 0% (w/v) to 16% (w/v). Then, we tested the stability of the mixing of those two materials to ensure no basic properties changed between them during the preparation of blend bioinks. The thermogravimetric (TGA) analysis and X-ray diffraction (XRD) analysis showed that there was no crystal structural change after grafting (Figure S4A–D, Supporting Information), confirming their stable physical and chemical structure during the synthesis process. Furthermore, these results from FTIR spectra (Figure S4E, Supporting Information), TGA (Figure S4F, Supporting Information), and XRD (Figure S4G, Supporting Information) analysis indicated that the mixture did not cause crystal structural changes.

2.2. Superiority of ϵ -PLMA in Alg-Based Bioinks

As depicted in Figure 1, in order to demonstrate the superiorities of our proposed polyelectrolyte – AlgMA/PLMA, three traditional Alg-based bioinks were chosen to compare with: i.e., Alg/ Ca^{2+} , the pure alginate which was post-crosslinked by Ca^{2+} (single molecule) after printing; AlgMA/ Ca^{2+} , the AlgMA which was post-crosslinked by UV light and Ca^{2+} after printing; AlgMA/GelMA, the mixture of AlgMA and large-molecule GelMA which was pre-crosslinked by electrostatic force before printing and post-crosslinked by UV light after printing. For the blend bioinks that we used, their operability in the preparation process should be considered, but often overlooked in the previous reports. To achieve a stable printing status, a uniform blend bioink is preferred. In order to compare the homogenization capacity of these bioinks, a stirring test was first carried out to compare the preparation performance of these four bioinks. Due to the twining of the long chain of GelMA and AlgMA, AlgMA/GelMA bioink needed at least double the time to homogenize than the other three bioinks. To further verify this phenomenon, we conducted semi-quantification experiments. AlgMA was stirred with GelMA-Rho (red fluorescent) and ϵ -PLMA-FITC (green

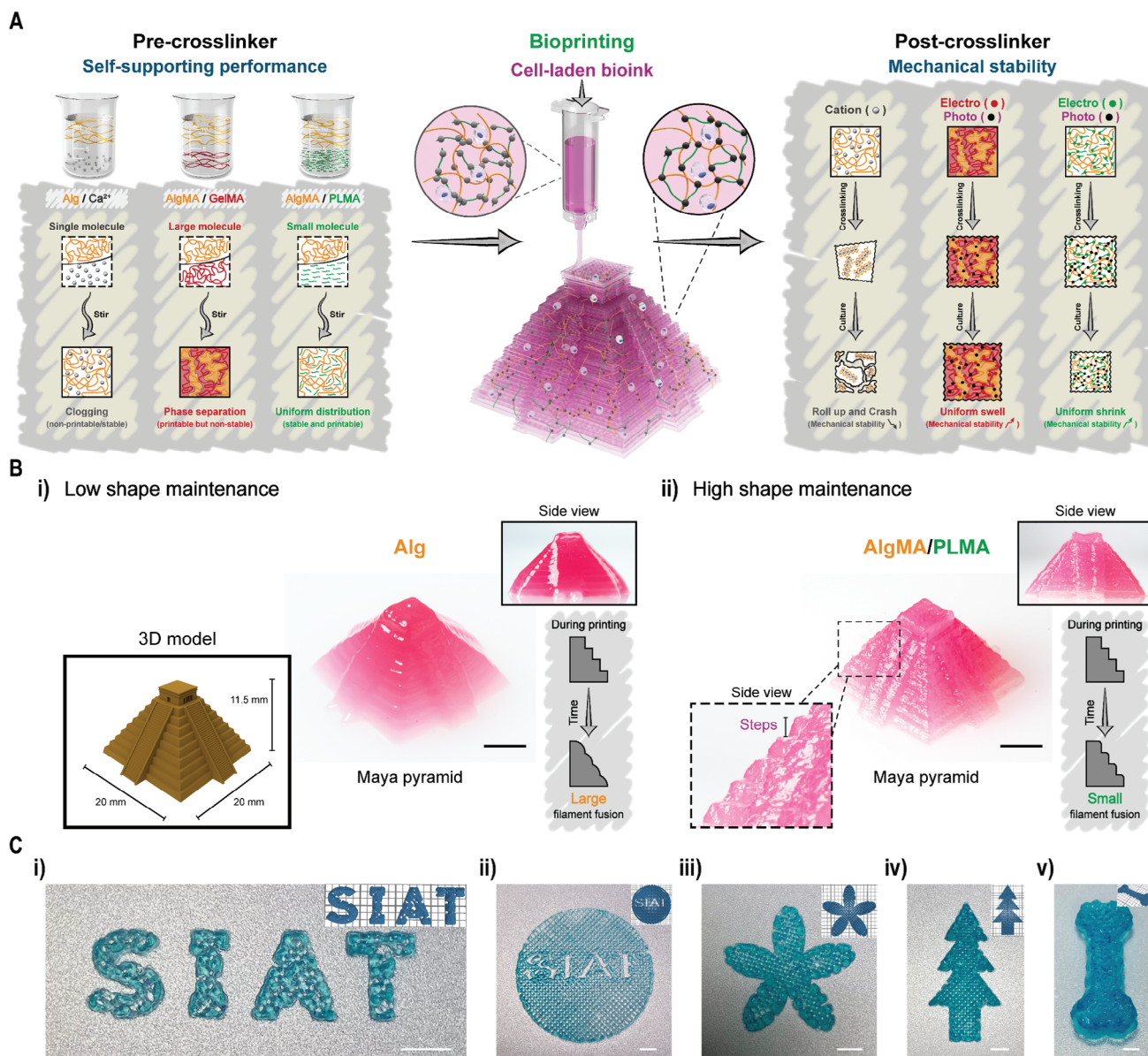


Figure 1. The schematic illustration of small molecular polycation used as crosslinker of bioink. A) The design of the bioink: AlgMA and ϵ -PLMA. B) The self-supporting property and shape maintenance of the AlgMA/PLMA bioink facilitate the successful fabrication of complex scaffolds – Maya pyramid. 17 × 17 × 11 mm (length × width × height). C) Physical images of large-size complex shape scaffolds printed by AlgMA/PLMA ink. Scale bar in B and C, 5 mm.

fluorescent), respectively, to reveal the micro-interactions between the two materials during mixture. As shown in Figure 2A and Figure S5 (Supporting Information), after as short as 10 s stirring, small-molecule ϵ -PLMA could be dispersed uniformly within AlgMA. However, when large-molecule GelMA was stirred with AlgMA to a relative uniformity, at least a 10 min mixing was needed (Figure 2A). Furthermore, through observing the new Nitrogen (N) element involved with ϵ -PLMA according to EDS assay, the uniformity of AlgMA/PLMA series inks (detailed formulations can be found in Table S1, Supporting Information) was evaluated. As shown in Figure S6 (Supporting Information), the blend materials had a uniform N element distribution and

showed a significant increment on N content with the increase of the ϵ -PLMA. Modulation of preparing time is important for bioinks, because the shorter mixing time, the less damage will be applied to the activity of cells. Based on the composites' homogenized dynamics, small-molecular pre-crosslinker has clear advantages over large-molecule additives.

Further, to compare the printability and crosslinking stability, we designed a “Ring—Hive” nested structure with neatly arranged hexagons surrounded by a ring. The printed structures of the AlgMA/GelMA and AlgMA/PLMA bioinks had precise hexagon outlines and the gaps between ring and hexagon were still visible after crosslinking (Figure 2B). In contrast, the ionic

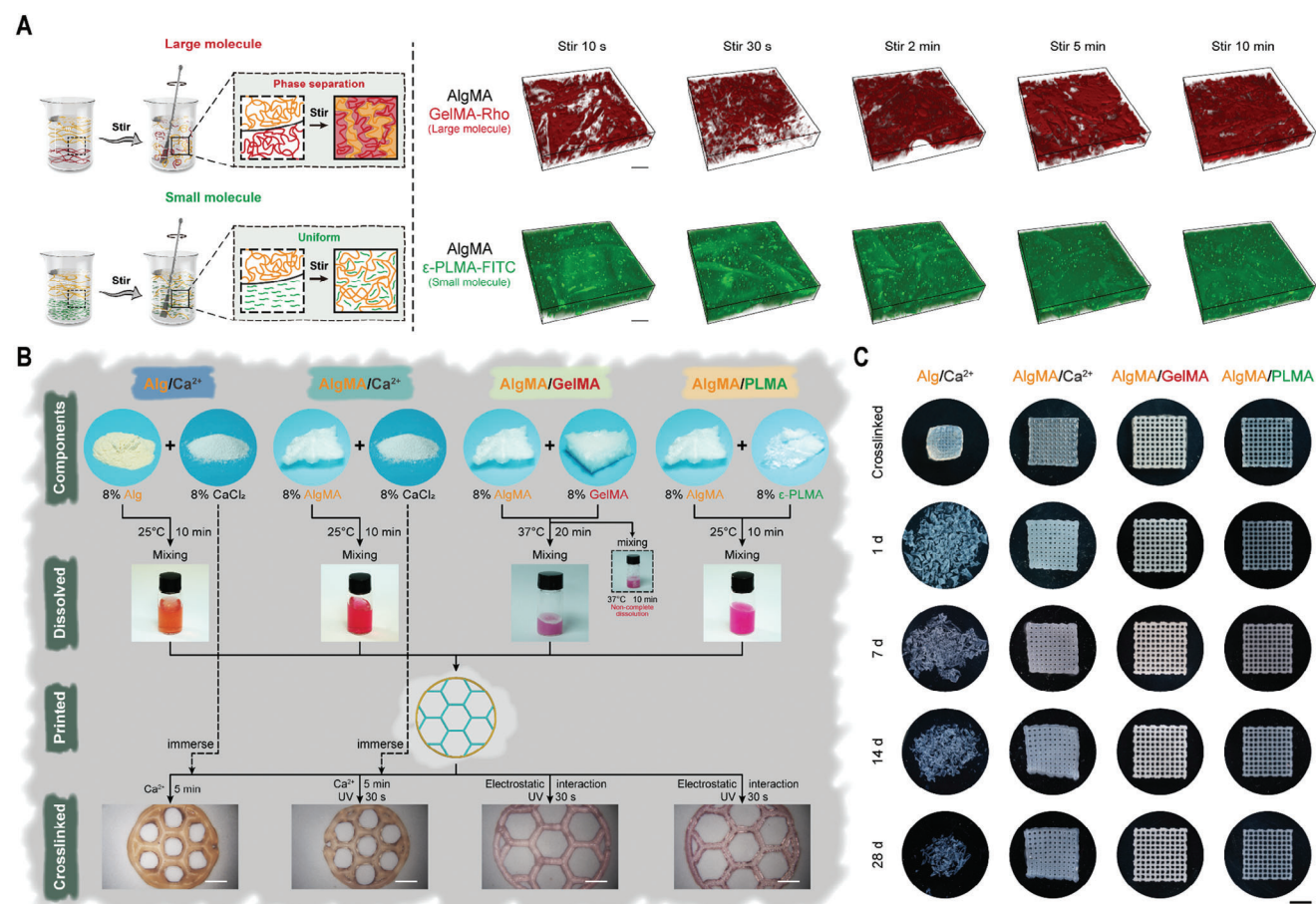


Figure 2. The preparation and crosslinking stability of Alg-based bioinks. A) Pre-gel AlgMA solutions containing different molecular-weighted crosslinkers have distinct performances during the mixing process. Scale bar in A, 50 μm . B) Preparation and 2D plotting of four kinds of Alg-based bioink. Scale bar in B, 2.5 mm. C) Macroscopic appearance of 3D-printed scaffolds at day 0 (Crosslinked), day 1, day 7, day 14, and day 28 of immersion in PBS (37 $^{\circ}\text{C}$, 60 rpm) for Alg/ Ca^{2+} , AlgMA/ Ca^{2+} , AlgMA/GelMA, and AlgMA/PLMA scaffolds. Scale bar in C, 5 mm.

crosslinking showed a blurry shape on the printed structure, suggesting that pre-crosslink is critical for keeping the fidelity of Alg-based ink. A long-time shape observation on the scaffolds immersed in PBS was conducted to further compare the stability of the four kinds of scaffolds. As shown in Figure 2C, the ionic crosslinking significantly deformed the scaffolds, while the electrostatic pre-crosslinking and photo post-crosslinking did not. After only 1 day, the physical structure of a single-crosslinked network by Ca^{2+} ion crushed, and the AlgMA/ Ca^{2+} scaffold shrank along with Ca^{2+} loss. The other two photo-crosslinked scaffolds maintained their structures for over 28 days (Figure 2C). Thus, a stable post-crosslinking is necessary for the Alg-based scaffold to meet its long-term request, e.g., in tissue engineering. As the results demonstrated in Figure 2B, the ϵ -PLMA enhanced the accuracy of Alg-based ink printing. However, to what extent can the capacity be? To figure it out, a “Criss-Cross” cubic structure with 90° rotated filaments of each layer was designed and printed for four layers. Figure 3A showed the printed grid-like scaffolds of Alg/ Ca^{2+} and AlgMA/ Ca^{2+} bioinks presented a massive structural collapse with time before crosslinking. Notably, the printed filaments of Alg/ Ca^{2+} and AlgMA/ Ca^{2+} bioink fused together in 10 s and 5 min post-printing, respectively. While the filaments

of AlgMA/GelMA and AlgMA/PLMA bioinks still maintained their shape within 5 min. This result demonstrates that Alg-based bioinks with pre-crosslinkers have more potential in large-scale bio-manufacture.

According to a previous report^[19] (Figure S7A, Supporting Information), the printing fidelity was usually defined as the matching degree of outline resolution (length \times width \times height) between the printed object and the designed model. In order to fulfill the printing structure outline, the Printability (Pr.) was carried out to describe the printing behavior.^[20] While for the detailed character of feature resolution (Figure S7B, Supporting Information), e.g., the steps of the pyramid (Figure 1B), most of the evaluation methods were qualitative. To detail the Alg-based hydrogels’ printing performances, we then defined several quantitative indexes, including Shape Maintenance (SM), Printing Stability (PS), and Crosslinking Stability (CS). Among them, SM and PS were evaluated during pre-crosslinking period, which provided the printed mesh size shrinkage over time and the uniformity of mesh size distribution, respectively. In contrast, CS was evaluated during post-crosslinking period, which provided the printed mesh deformation over time during post-crosslinking period.

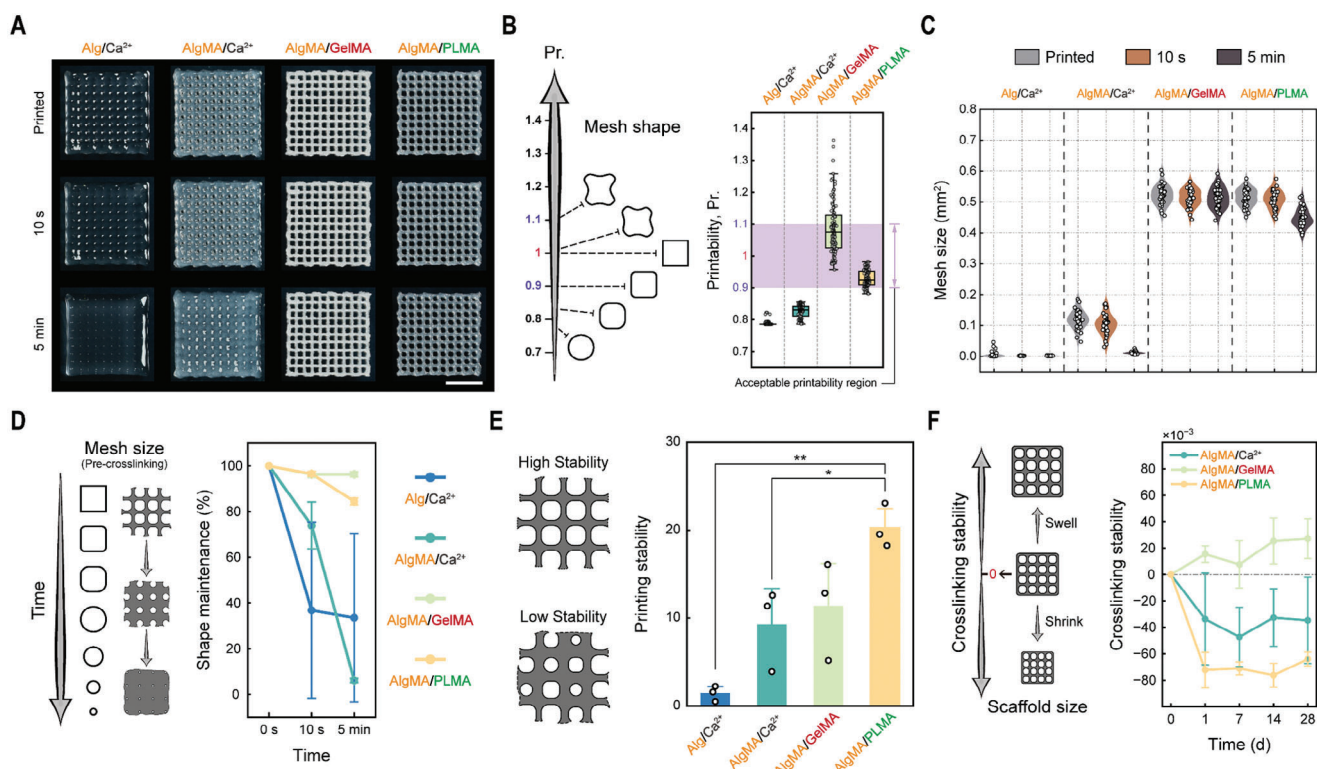


Figure 3. The printing performance of Alg-based bioinks. A) The shape changing of filaments with time after Alg-based scaffolds are manufactured. Scale bar in A, 5 mm. B) Printability (Pr.) of four Alg-based scaffolds. C) Mesh size of four Alg-based scaffolds of just printed, 10 s after printed and 5 min after printed. D) Shape maintenance of four kinds of Alg-based bioink. E) Printing stability of four kinds of Alg-based bioink. F) Crosslinking stability of AlgMA/GelMA and AlgMA/PLMA scaffolds. ($n = 3$, $*p < 0.05$, $**p < 0.01$, $***p < 0.001$).

First, Pr., calculated as Equation 1 and 2, was used to illustrate the printing behavior of different bioinks. According to a previous report,^[20] when the Pr. is in the range of 0.9–1.1, the 3D printed hydrogel construct should demonstrate fine-filament morphology and be mechanically stable. As shown in Figure 3A, the four bioinks printed grids had different mesh shapes, respectively. The mesh shapes of Alg/Ca²⁺ and AlgMA/Ca²⁺ were circle and rectangle with chamfers, reflecting on the Pr. Values were 0.79 and 0.83 (Figure 3B), respectively; the mesh shapes of AlgMA/GelMA and AlgMA/PLMA were irregular polygon and clear rectangle (Figure S8A, Supporting Information), with the Pr. Values of 1.09 and 0.93 (Figure 3B), respectively. Although these two pre-crosslinked bioinks achieve acceptable Pr., the filaments of AlgMA/PLMA bioink showed a smoother surface than AlgMA/GelMA bioink (Figure S8A, Supporting Information).

During the manufacture of large-scale constructs, the filaments need to maintain their shape for a long time. Otherwise, the printed filaments will present displacement, which causes progressive dislocation, thus blurring the steps of the pyramid. Taking the comparison between Alg ink and AlgMA/PLMA ink as an example, the 7th – 8th step angle and 3rd – 4th step angle of designed 3D model is 104°. Due to surface tension and the low stability of Alg ink, the filaments between these steps lost protruding parts and fused together, resulting in a smooth surface. While AlgMA/PLMA ink maintained the feature resolution of the pyramid (Figure S7B, Supporting Information),

with the angles of 7th – 8th step angle and 3rd – 4th step were 109° and 135°, respectively. As a new evaluation parameter, SM was identified with Equation 3 to further discover this property. By counting and analyzing the mesh size of the four scaffolds, these two pre-crosslinked bioinks showed better performance on SM (Figure 3C,D). As shown in Figure 3D, at 10 s after printing, SM of both of the polyelectrolyte bioinks could achieve ≈ 97%, which were 37% and 74% for the Alg and AlgMA electrolyte bioinks, respectively. With time extended to 5 min, SM of Alg/Ca²⁺, AlgMA/Ca²⁺, AlgMA/GelMA and AlgMA/PLMA bioinks changed into 33.5%, 6.1%, 96.3%, and 84.4%, respectively. The slight change between 10 s and 5 min of Alg/Ca²⁺ was because the filaments started to fuse immediately after the second layer was printed. The slight advantage of AlgMA/GelMA bioinks over AlgMA/PLMA bioinks was caused by the physical crosslinking in the room temperature of GelMA.

The successful manufacture of a large structure not only needs the SM of each filament, but also the uniformity of each filament. In other words, the mesh size should be kept in a narrow range. PS, as another parameter, was carried out to further analyze this scaffold mesh variation phenomenon that reflects the stability of printed filaments. The printed mesh size uniformity was evaluated by calculating the proportion of the average mesh size (A_{MS}) and the value's standard deviation (S_{MS}), as shown in Equation 4, 5, and 6. From Figure 3E, the PS of Alg/Ca²⁺, AlgMA/Ca²⁺, AlgMA/GelMA, and AlgMA/PLMA bioinks were 1.45, 9.28, 11.37, and 20.29, respectively, meaning that the

AlgMA/PLMA bioink has the highest printing stability among these Alg-based bioinks.

Finally, after successfully manufacturing a large-scale structure, how long and how accurately will this object maintain its shape with the help of post-crosslinker? Since the crosslinked printed object needs to maintain its shape to perform functions, another parameter – CS, was introduced. A long-time shape observation on the scaffolds immersed in PBS was conducted to evaluate the post-crosslinkers' performance. After calculating with Equation 7 and 8, the CS resulting from ion crosslinker – Ca^{2+} , and covalent crosslinker – MA were analyzed, respectively. As shown in Figure 3F; Figure S8B,C (Supporting Information), AlgMA/ Ca^{2+} and AlgMA/PLMA scaffolds presented a slight size shrinkage reflecting CS values from 0 to -0.034 and -0.072 on 1-day post-printing, respectively. In contrast, AlgMA/GelMA scaffolds presented a little swell on the size, reflecting CS value from 0 to 0.015. After that, all three inks showed a stable scaffold size under a long-time incubation (28 days).

Collectively, these results indicate that the AlgMA/PLMA bioink based on a small-molecule pre-crosslinker has the best printing performance among those four kinds of bioinks. Moreover, it is worth noting that, the isometric shrinkage on the AlgMA/PLMA scaffold size without changing the original shape could be applied in high-precision additive manufacture.^[21] Indeed, the AlgMA/PLMA can print complex structures with high accuracy, such as a large-sized bone with a certain thickness.

2.3. Printability of AlgMA/PLMA Bioinks

Due to the high printability and application potential in tissue engineering of the small-molecule pre-crosslinker-based AlgMA/PLMA ink, we further characterized the physicochemical properties of different series of AlgMA/PLMA as bioinks (Table S1, Supporting Information). As mentioned before, we prepared a series of AlgMA/PLMA polyelectrolyte bioinks by fixing AlgMA content to 8% (w/v) and increasing ϵ -PLMA content from 0% (w/v) to 16% (w/v) for investigation.

Charge property is very important for biomaterials, as for different sorts of cells, their preferred potential is totally different. After characterizing this property, we surprisingly found that the surface potential of the AlgMA/PLMA series materials increased with the content of ϵ -PLMA on similar surface roughness (Figure 4A,B). The surface potential increased from -345.25 mV to 121.55 mV with the increase of ϵ -PLMA from 0% to 16%. Obviously, involving positively charged small molecular ϵ -PLMA could change the electrical microenvironment of Alg-based materials. Another property that has a significant influence on cell behavior is hydrophilicity. It can be seen from Figure 4C that from AlgMA8 to AlgMA8-PLMA16, the surface water contact angles (WCA) of the materials increased from 26.64° to 52.00° . The introduction of ϵ -PLMA neutralized the AlgMA negative charges, e.g., $-\text{COOH}$, leading to reduced hydrophilicity and water absorption. In addition, the increased surface electric potential with the increase of ϵ -PLMA was also one of the reasons for hydrophilicity decrease, which was also reported by Xu et al.^[22] As previously reported, the biocompatible water contact angle is 40° – 70° .^[23] Thus, by adjusting PLMA content, the AlgMA/PLMA materials can obtain the bio-favorable hydrophilicity. Besides affecting the

inaction with cells, the hydrophilicity level also determines hydrogel shape deformation due to high-water absorption. During tissue engineering application, the scaffold usually needs long-time culture, thus the stability in an aqueous environment is quite an important property. Here, we measured the water absorption (WA) and degradation to evaluate the AlgMA/PLMA material's durability (Figure 4D,E). It can be seen from Figure 4D that the AlgMA8 hydrogel severely swelled when immersed in PBS for 1 h, and reached the swelling equilibrium state until 36 h, with a final WA rate at 13.06%. The ionization of the $-\text{COOH}$ groups in the AlgMA molecular chain promotes water to diffuse into the polymer network, resulting in AlgMA hydrogel swelling. While, all hydrogels containing ϵ -PLMA reached swelling equilibrium within 2 h; with the increase of cationic crosslinker ϵ -PLMA content, the equilibrium water swelling rate of AlgMA/PLMA hydrogel also decreased. Interestingly, at the 3rd hour of incubation, the weight of all AlgMA/PLMA materials declined.

In addition to the neutralized hydrophilic groups, the hybrid material has more crosslinking sites and a denser network, restricting water entry and swelling, which could be another reason for the decrease of the hydrophilicity. The SEM image in Figure S9 (Supporting Information) also supports this speculation. Figure S9 (Supporting Information) shows that, the pore structure of hydrogel began to shrink after the introduction of the cationic crosslinking agent ϵ -PLMA; and with the increase of the positive to negative charge ratio, the crosslinking density of the AlgMA/PLMA series hydrogel increased, and the formed network became denser, resulting in smaller pore size. As for AlgMA8-PLMA16, the pore size of its cross-section is even smaller than $20\ \mu\text{m}$, which limits cell growth and nutrition exchange. However, ϵ -PLMA not only crosslinks with AlgMA, but also presents self-crosslinking. The scaffold with a higher ratio of positive to negative charges contained more ϵ -PLMA, and the self-crosslinked ϵ -PLMA particles deposited on the surface of the scaffold (Figure S9A, Supporting Information), which was continuously oscillated by PBS, resulting in a weight decrease. After that, the scaffold would reach a new swelling equilibrium state, as shown in Figure 4D. Therefore, less water absorption gives AlgMA/PLMA ink relatively excellent structural fidelity and dimensional stability. The results illustrate that AlgMA/PLMA ink has a low degree of water absorption (WA), which could not only prevent the scaffold from losing the structural accuracy obtained by 3D printing, but also avoid damaging the tissue defect site and causing secondary injury.

Degradation behavior is another critical factor in evaluating biomaterial properties in maintaining structural integrity during long-time application scenarios. The degradation of each AlgMA/PLMA material within 7 days of culture is demonstrated in Figure 4E. It can be seen that the AlgMA8 hydrogel barely degraded in the early stage, and it began to degrade slowly on the 4th day. It was speculated that the AlgMA material formed a single network structure after UV photo-crosslinking, which was relatively stable in the early stage. However, it was affected by the high hydrophilicity of AlgMA, and a large number of water molecules entered the network structure of the scaffold in the early stage. As a result of AlgMA hydrolysis, the mass of AlgMA8 scaffolds began to lose. However, the scaffold containing ϵ -PLMA experienced mass loss in the first 2 days, and then entered a plateau stage; and the AlgMA/PLMA scaffold also degraded

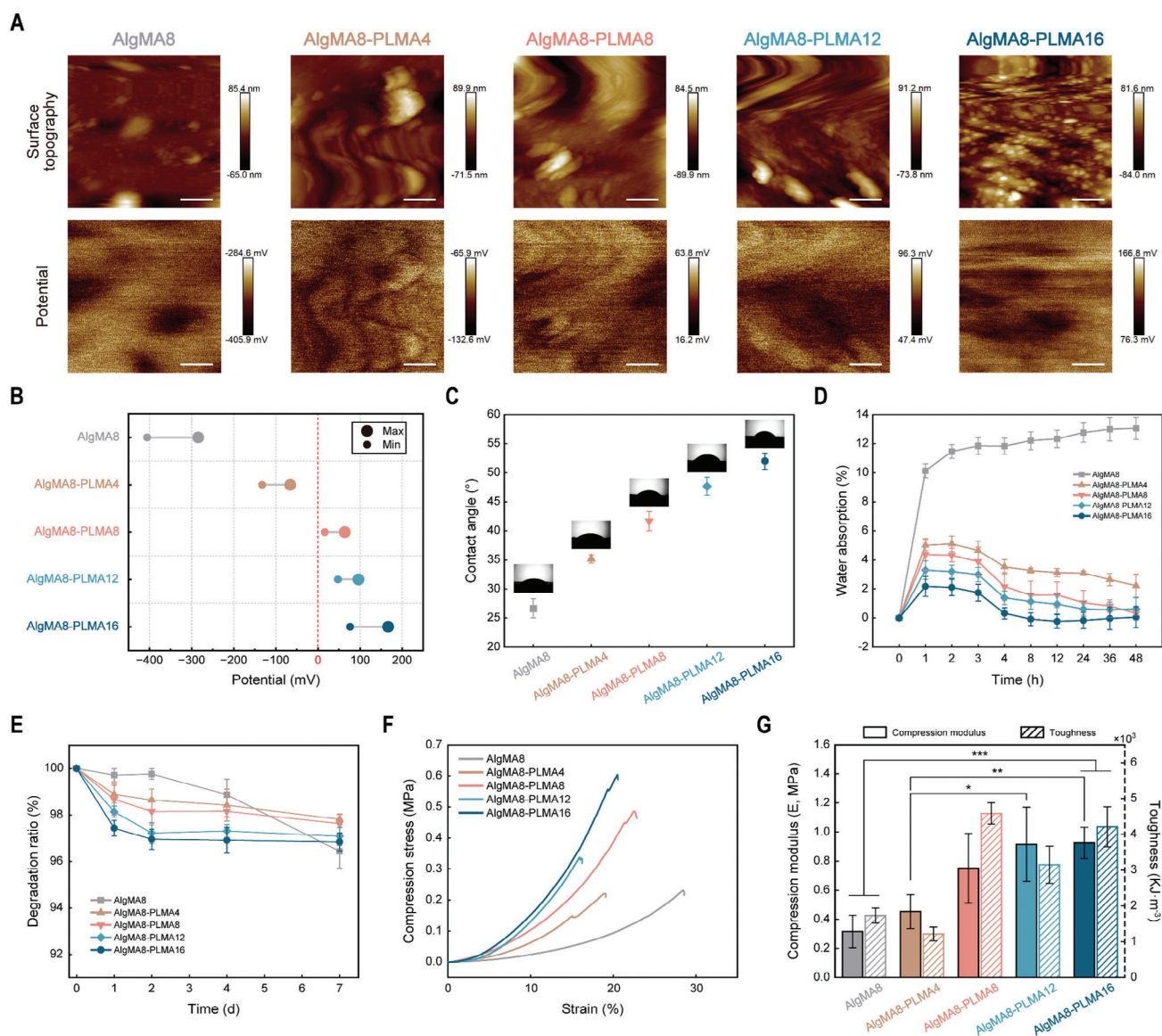


Figure 4. The physical properties of AlgMA/PLMA bioink. A) Surface topography and potential of AlgMA/PLMA. Scale bar in A, 400 μm . B) Influence of ϵ -PLMA concentration on the potential range of AlgMA/PLMA materials. C) Water contact angle diagram of different ratio of AlgMA/PLMA. D) Water absorption ratio of different ratio of AlgMA/PLMA within 48 hours. E) Degradation test of different ratio of AlgMA/PLMA within 7 days. F) Compression mechanical properties of different ratio of AlgMA/PLMA. G) Compression modulus and toughness of different ratio of AlgMA/PLMA. ($n = 5$, $*p < 0.05$, $**p < 0.01$, $***p < 0.001$).

more in the early stage with the increment of ϵ -PLMA (Figure 4E). The early mass loss was due to the small molecule ϵ -PLMA self-crosslinking network deposited on the surface of the scaffold, which was washed out by the PBS solution during constant oscillation until it fell off completely. Then, the effects of ϵ -PLMA on AlgMA hydrogels' mechanical properties were measured. It can be seen from the compressive stress-strain curve that as the ratio of positive to negative charges increased, the compressive strength of the hydrogel also increased (Figure 4F). The strong electrostatic interaction between the charges highly contributes to the enhanced mechanical properties of the AlgMA/PLMA hydrogel. It was found that the compressive strain of the AlgMA8

hydrogel is the largest. The compressive modulus plot showed that from AlgMA8 to AlgMA8-PLMA16, the compressive moduli of the scaffold increased with ϵ -PLMA content, which were 0.317, 0.454, 0.751, 0.916, and 0.926 MPa, respectively (Figure 4G). Thorough calculation, the toughness of AlgMA/PLMA hydrogels were 1731, 1218, 4583, 3152, and 4210 KJ m^{-3} , respectively (Figure 4G). From the SEM data, the decrease in elasticity with the introduction of the cationic crosslinking agent ϵ -PLMA could be explained. The crosslinking density of the scaffold became higher, and the double network structure combined more (Figure S9, Supporting Information), thus increasing the brittleness of the hydrogel. This is because the greater the crosslinking density

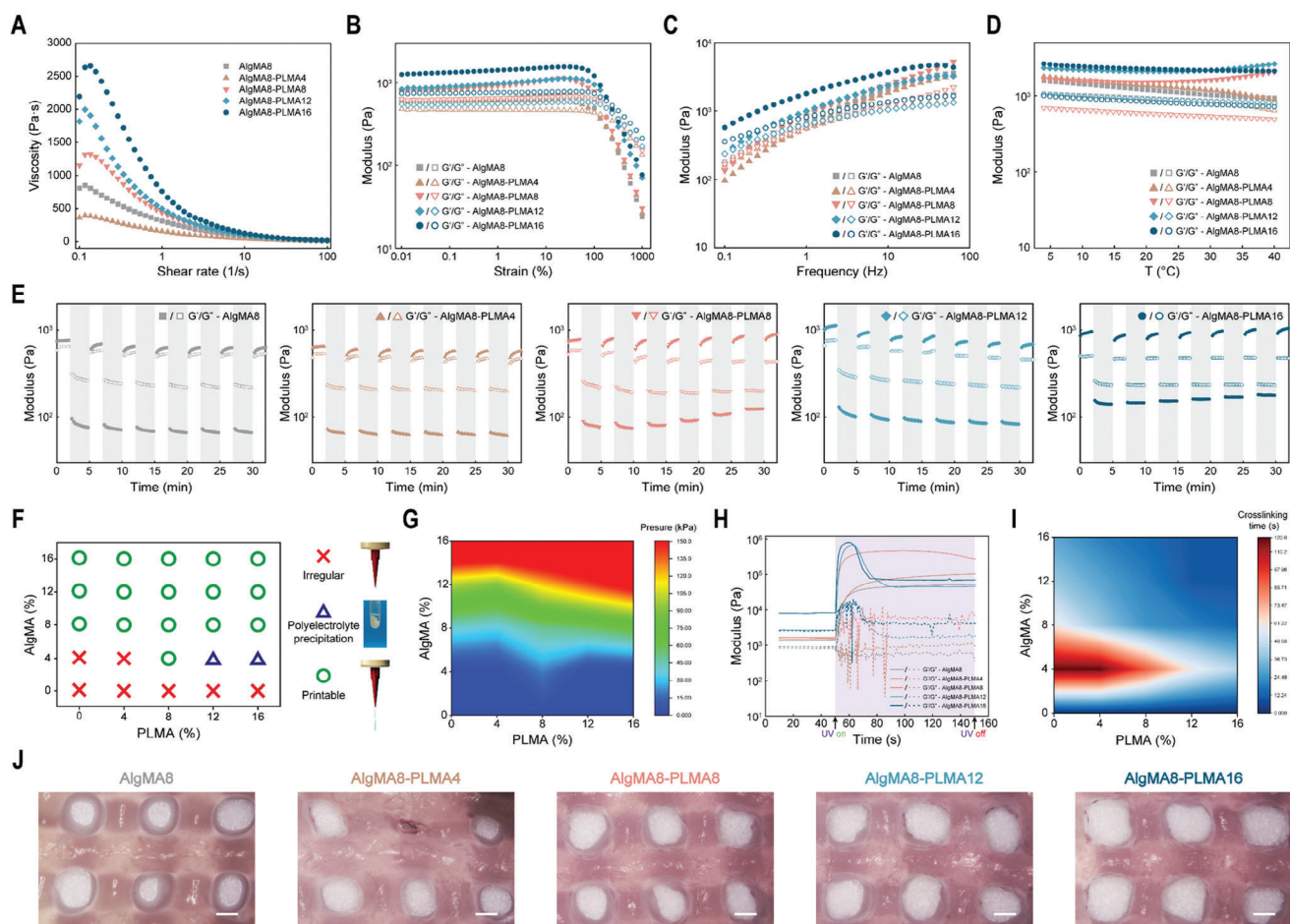


Figure 5. The printability of AlgMA/PLMA bioink. A) Influence of shear rate ($0.1\text{--}100\text{ s}^{-1}$) on the viscosity of AlgMA/PLMA. B) Influence of strain ($0.01\text{--}1000\%$, 1 Hz , $25\text{ }^{\circ}\text{C}$) on the storage/loss modulus (G'/G'') of AlgMA/PLMA. C) Influence of frequency ($0.1\text{--}100\text{ Hz}$, 1% strain, $25\text{ }^{\circ}\text{C}$) on the storage/loss modulus (G'/G'') of AlgMA/PLMA. D) Influence of temperature ($4\text{--}40\text{ }^{\circ}\text{C}$, 1% strain) on the storage/loss modulus (G'/G'') of AlgMA/PLMA. E) Shear-thinning and self-healing behavior test. Influence of strain-cycle (low: unshaded, 1% strain, 1 Hz and high: shaded, 500% strain, 1 Hz) on the (G'/G'') of AlgMA/PLMA. F) The analysis of extrusion status of different ratio of AlgMA/PLMA. G) The extrusion pressure of different ratio of AlgMA/PLMA in heat map. H) Influence of UV exposure time ($1\text{--}100\text{ s}$, 1% strain) on the storage/loss modulus (G'/G'') of AlgMA/PLMA. I) The photo-crosslinking time of different ratio of AlgMA/PLMA in heat map. J) Effect of different ratios on the accuracy of structure for AlgMA/PLMA scaffolds. Scale bar in J, $400\text{ }\mu\text{m}$.

of the polymer, the greater the bonding force between its molecular chains, and the harder it is to deform it by an external force.

For extrusion printing, the ink's rheological properties are tightly linked to its printability, helping to set printing parameters. In order to find the best printing window of AlgMA/PLMA series inks, the rheological test was performed to assist. **Figure 5A** exhibited the shear-thinning behaviors of the AlgMA/PLMA series inks. At a low shear rate of 0.1 s^{-1} , the addition of ϵ -PLMA increased the mixtures' viscosities from 0.810 to 21.948 kPa s . Then, along with shear rate speeding, the mixtures' viscosities first underwent a slight increase, followed by a continuous decline, representing good shear-thinning properties. The small rising zone at the beginning is highly due to the unwinding of the AlgMA long-chain polymer. Usually, the strain required for the solid-liquid phase transition of the ink relates to the printing pressure. It can be seen from **Figure 5B** that with the increased strain, the moduli of all AlgMA/PLMA series bioinks decreased, and a phase transition occurred, indicating that the bioink will

transform from a solid state to liquid under extrusion pressure ($G' < G''$). The phase transition point of the AlgMA/PLMA series inks can be observed by locally zooming in the modulus-strain curve in the range of 35% to 350% . It can be seen from the figure that with the introduction of cationic crosslinker ϵ -PLMA, the yield strains of AlgMA/PLMA series inks were also increased. Corresponding to the printing process, the extrusion pressure of the bioink increased with the increasing ratio of positive to negative charges. Nevertheless, the phase transition points of AlgMA/PLMA series inks were generally lower than 300% strain, indicating the inks can be extruded under cell-friendly pressure. To observe the influence of the printing air pressure loading frequency on the extrusion performance of the non-Newtonian fluid ink, the "modulus-frequency" rheological test was carried out. It can be seen from **Figure 5C** that the frequency had a specific influence on the moduli of AlgMA/PLMA inks, reflecting the influence of the printing interval on the rheological properties of the inks. That is, the lower the frequency, the fewer times

the bioink can be squeezed out within a specific period of time. Figure 5C shows that the liquid-to-solid phase transition point of most bioinks occurred at a low frequency of ≈ 1 Hz, that is, during the regular 3D printing air pressure application and removal process (generally less than 1 second to switch the air pressure once), the phase transition of the AlgMA/PLMA ink usually occurred. To determine the optimal printing temperature, the “modulus-temperature” screening was carried out. As shown in Figure 5D, the temperature between 4 °C and 40 °C had a negligible influence on the moduli of AlgMA/PLMA series inks, demonstrating the printing stability of the inks (Figure 5D). As is well known, a wide temperature range is a considerable advance for bioprinting, since the printing can be processed either in ambient temperature when lacking plug-in-heater, or at 4 °C or 37 °C to enhance the cell viability or metabolism depending on the research purpose. Ink experiences “pressure on/off” cycles during pneumatic extrusion printing. To simulate this process, a “Cyclic Oscillation” test was performed. Figure 5E showed that under high strain, all AlgMA/PLMA bioinks exhibited liquid behavior ($G' < G''$), consistent with Figure 5B results; when the stress was removed, all bioinks quickly recovered and exhibited solid state behavior. And with the increase in the number of cycles, the moduli of all bioinks can be maintained within a certain range, indicating that the AlgMA/PLMA bioinks had self-healing behavior, self-supporting behavior, and good printing stability.

After characterizing the printability of AlgMA/PLMA bioinks via rheological test, an on-machine test was carried out to confirm the results. By extruding the bioinks through a 3D printer (Bio-Architect WS, Regenovo), the status of filaments and printing pressure were recorded for future analysis. It can be seen from Figure 5F and Figure S3B (Supporting Information) that ϵ -PLMA alone was unprintable, and so did AlgMA4 and AlgMA4-PLMA4 bioinks. Because these bioinks were so dilute, the inks dripped out of the needle when placed in a vertical printing barrel without applying pressure. Besides AlgMA4-PLMA12 and AlgMA4-PLMA16, no precipitation occurred in other ink formulations, meaning that when the ratio of positive to negative charges is greater than 3:1, AlgMA/PLMA bioinks will produce polyelectrolyte precipitation (Figure S3B, Supporting Information). As a result, only AlgMA/PLMA bioinks with 8%, 12%, and 16% (w/v) ϵ -PLMA were eligible for printing. It can be seen from Figure 5G and Figure S3C (Supporting Information) that the printing pressure was mainly controlled by AlgMA content. Especially when fixing the AlgMA to 8% (w/v), the pressures keep constant regardless of ϵ -PLMA changes. To further confirm the performance of the post-crosslinker (i.e., MA) quantitatively, a rheological test in “UV cure” mode was performed on the UV cure capability of the ink. It can be seen from Figure 5H that all AlgMA/PLMA bioinks can be quickly cured by UV photo-crosslinking within 10 s, and the elastic moduli raised along with ϵ -PLMA content increase. Interestingly, thereafter, the elastic moduli of AlgMA-PLMA12 and AlgMA-PLMA16 hydrogels suffered from a 20 s decrease. During UV crosslinking, AlgMA-PLMA12 and AlgMA-PLMA16 formed denser networks than the other three hydrogels, which squeezed out more water. The declining phenomenon was likely caused by a water-mediated lubrication layer between the stiff hydrogel and the rheometer flat plate. The addition of ϵ -PLMA will increase the crosslink density of AlgMA/PLMA ink and make the hydrogel stiffer. The crosslinking time decreased for the higher density

of the double bond (Figure 5H,I, and Figure S3D, Supporting Information).

Through an extrusion-based 3D printer, the AlgMA/PLMA bioinks were used to construct the scaffolds, and the influence of different charge ratios on the structural accuracy was explored. It can be seen from Figure 5J, Figure S3E and Figure S9C (Supporting Information) that the scaffolds except the AlgMA8-PLMA8 group can maintain a good cross-structure accuracy; and as the ratio of positive to negative charges increased, the pores of the scaffold became larger, indicating that the addition of cation coupling agent ϵ -PLMA will make the scaffold lines more tightly cured; while the AlgMA8-PLMA4 bioink had low viscosity, and occasionally the pores collapsed when constructing the scaffold. The initial introduction of the cationic crosslinking agent ϵ -PLMA will destroy the stability of the negative charge environment of the ink, and the charge neutralization occurred, resulting in a decrease in the viscosity of the bioink. However, as the ratio of positive to negative charges continued to increase, the charge neutralization reached equilibrium, it began to become a positively charged environment (Figure 4A), so the viscosity increased continuously with the increase of solid content. During the mixing process, compared with AlgMA8 ink, AlgMA8-PLMA4 was easier to stir and AlgMA8-PLMA8 cost more effort, which was consistent with the viscosity-shear rate rheological test results.

With the increase of AlgMA solid content, the printing pressure increased while crosslinking time decreased significantly. Applied as cell printing ink, high shear force and irradiation of cells with UV light will cause cell membrane destruction and risk of DNA fragmentation and mutation. For example, when the AlgMA content was too small, the ink could not be printed (Figure 5F); as the AlgMA content increased, the printing extrusion pressure also increased significantly; and when the ratio of positive to negative charges was too large, polyelectrolyte precipitation will occur; conversely, the photo-crosslinking time of the ink will increase. Indicating that a well-optimized formulation of polyelectrolyte ink (herein AlgMA/PLMA) is essential to maximize its advantages in bioprinting.

2.4. Regulation of Cell Behaviors via The Charge Of Bioinks

During biomedical applications, thus as tissue engineering and organoid, extracellular matrix plays critical roles in governing cell fate. Developed as a kind of bioprinting ink, the AlgMA/PLMA has proved its ability in precise construction. Then, uncovering its interaction with cells is an essential step.

Due to its accessibility, multi-lineage differentiation capacity, and paracrine trophic and microenvironment regulation potential, mesenchymal stem cells (MSCs) are widely studied in pre-clinical research and clinical trials.^[24] We first introduced bone marrow-derived MSCs (BMSCs) into the AlgMA/PLMA inks (designated as AlgMA/PLMA-BMSC) and further explored the interaction between cells and AlgMA/PLMA inks. The rheological test revealed that $1 \times 10^6 \text{ ml}^{-1}$ cells have a negligible effect on the ink viscosity (cell-free: 4.57 kPa s under 0.1 s^{-1} and $1 \times 10^6 \text{ ml}^{-1}$: 4.08 kPa s under 0.1 s^{-1}), which continuously decreased to 1.12 kPa s with the increase of cell density to $20 \times 10^6 \text{ ml}^{-1}$ (Figure S10A, Supporting Information). Accordingly, the ink G' showed negligible influence under $1 \times 10^6 \text{ ml}^{-1}$ cells (cell-free:

17.0 kPa under 0.1% strain and $1 \times 10^6 \text{ ml}^{-1}$: 15.2 kPa under 0.1% strain), which continuously decreased to 2.8 kPa with the increase of cell density to $20 \times 10^6 \text{ ml}^{-1}$ (Figure S10B, Supporting Information). The phenomenon is consistent with that previously reported that a high density of cells will reduce the hydrogel G' and viscosity because of the interrupted polymer chain interaction.^[25] On the other hand, high cell density benefits tissue construction. Thus, bioprinting is a balance of cell concentration and ink printability. In our study, to ease the observation of BMSC proliferation and spreading behavior, low cell density (i.e., $2 \times 10^6 \text{ ml}^{-1}$) was chosen to prepare printing ink. During the printing process, the cells suffer from shear stress, controlled by nozzle type and diameter, printing pressure, and ink viscosity.^[26] Our results demonstrate that the BMSCs within AlgMA/PLMA were more sensitive to nozzle type instead of printing pressure (Figure S10C,D, Supporting Information). For example, using a tapered nozzle, the cell viability of AlgMA8-PLMA8-BMSC bioink decreased from 84.80% to 77.37%, when printing pressure increased from 45 to 100 kPa, which is 51.59% to 23.71% with straight nozzle. The higher inner shear stress within a straight nozzle contributed to the differences.^[27]

Thereafter, the AlgMA/PLMA-BMSC bioinks were printed with a tapered nozzle under 45 kPa. As the bioinks have different viscosity, the printing speeds were optimized to match their feeding speeds (Table S2, Supporting Information). After printing, the cell viability, proliferation, and spreading were measured to evaluate how the AlgMA/PLMA scaffolds modulate BMSCs behaviors (Figure 6A–E). As early as 4 h post-printing (named as day 0), the BMSCs in the AlgMA/PLMA scaffolds showed different survival situations, which were 71.05%, 75.69%, 84.80%, 85.87%, and 83.21%, respectively, indicating PLMA (Figure 6A-left panel, and 6B). However, during the subsequent culture period, the cells in AlgMA8 and AlgMA8-PLMA4 died massively, especially for the AlgMA8 group (approximately 90% dead) (Figure 6B,E). AlgMA8-PLMA8 ink maintained the high viability and proliferation of BMSCs through the 7 days assessment, while AlgMA8-PLMA12 and 16 inks did not. Although cell numbers in AlgMA8-PLMA8, 12, and 16 were similar on day 4 post-printing, EdU staining results show that the cell proliferation rates slowed down with PLMA increase (Figure 6A-right panel; Figure S11A,B, Supporting Information). Consequently, on day 7, the number of BMSCs in AlgMA8-PLMA12 and 16 decreased, especially for that in AlgMA8-PLMA16, which was even less than on day 4. We still need to find out the exact mechanism of the observed phenomenon. As shown in Figure S9B (Supporting Information), the smaller pore size, restricting the nutrition and oxygen exchange, may cause the differences.^[28]

Cell functionality is highly related to its spreading situation.^[29] Herein, we studied BMSCs spreading within AlgMA/PLMA scaffolds after 4 and 7 days of culture (Figure 6A-middle panel; Figure S11C, Supporting Information). Owing to the bio-inertness of alginate material, BMSCs within pure AlgMA were round or ellipse-shaped. With the introduction of the cationic PLMA, BMSCs started to spread, containing more pseudopodia. Interestingly, contrary to the proliferation results, BMSCs spreading areas were positively correlated to the PLMA content (Figure 6D). Within AlgMA8-PLMA4, the BMSCs exhibited short spindle shapes. With the PLMA increased to 8%, 12%, and 16% (w/v), more cells tend to have filopodia-rich morphology, stretched spin-

dle shapes, and large polygonal shapes, respectively. Increasing PLMA content enhanced AlgMA/PLMA network crosslinking density. The morphology changes are likely a consequence of BMSCs responding to surrounding materials with different stiffnesses.^[30]

With the progress of 3D bioprinting, scientists have started to fabricate more complex structures, e.g., an organ, which requires the ink enables to replicate the structural details, and also serve as a multicell niche. Thus, we also evaluated Schwann cells (SCs) to further extend the AlgMA/PLMA inks' border in nerve regeneration (Figure 6F–J). As aforementioned, grafting cell adhesion motifs, e.g., RGD, or hybrid with material that has cell adhesion sites, e.g., gelatin-based materials, are classic strategies to enhance alginate biofunction. In Figures 2 and 3, we have compared the effects of PLMA and GelMA on AlgMA operability and stability. Hereafter, the AlgMA/GelMA-SC was enrolled into the study array to evaluate the AlgMA/PLMA property as a bioprinting ink comprehensively.

Consistent with BMSCs, SCs grew well within the AlgMA/PLMA scaffolds (Figure 6F–J). However, the two cells had different responses to the AlgMA/PLMAs. For instance, unlike BMSCs, SCs within the AlgMA8-PLMA4 showed slightly higher viability than that in AlgMA8-PLMA8, 12, and 16 (Figure 6F-left panel and 6G). Interestingly, the SCs within AlgMA8-PLMA4 started proliferation more quickly, and were then surpassed by the SCs within the other three AlgMA8-PLMAs scaffolds (Figure 6J). The EdU staining on the 4th day post-printing demonstrated this proliferation switch phenomenon (Figure 6F-right panel). This result is somewhat surprising because material surfaces enriched with amine groups usually improved the proliferation of SCs. For example, Wang et al. compared the effects of different surface groups on SCs behaviors, and found that the glass coverslips grafted with amino groups resulted in more SCs adhesion and proliferation than carboxyl groups.^[31] As shown in Figure 6F,J; Figure S12A,B (Supporting Information), on the 1st and 4th days post-printing, the PLMA content was negatively correlated to the lower cell number, while on the 7th day post-printing, the two are positively correlated. Thus, the SCs proliferation capacity in AlgMA8-PLMA8, 12, and 16 scaffolds is more likely postponed instead of inhibited. We hypothesize that the phenomenon is a result of different cell-material interaction. As Lee and colleagues reported, the strength of cell adhesion on NH_2 -terminated surfaces was nearly an order of magnitude higher than on the RGD-terminated surface.^[32] So, during the first 4 days, strong electrostatic interaction between the SCs and amine groups on the AlgMA8-PLMA8, 12, and 16 surfaces slowed down cell proliferation, thereafter, as the positive material surfaces absorbed more protein from the culture media, the ligand-receptor interaction took into the dominant position, resulting in enhanced proliferation.

As shown in Figure 2A, the AlgMA8-GelMA8 ink cost 10 min of stirring to have similar uniformity with AlgMA8-PLMA8 ink. When cells were involved, the long-time mixing process caused significantly higher cell death (Figure 6F-left panel and 6G). Even though, the SCs within the AlgMA8-GelMA8 scaffold continuously proliferated during the following culture times (Figure 6J). Figure 6A-middle panel, Figure 6I, and Figure S12C (Supporting Information) depict the SCs spreading in the AlgMA/PLMA series and the AlgMA8-GelMA8 scaffolds after 4 and 7 days of

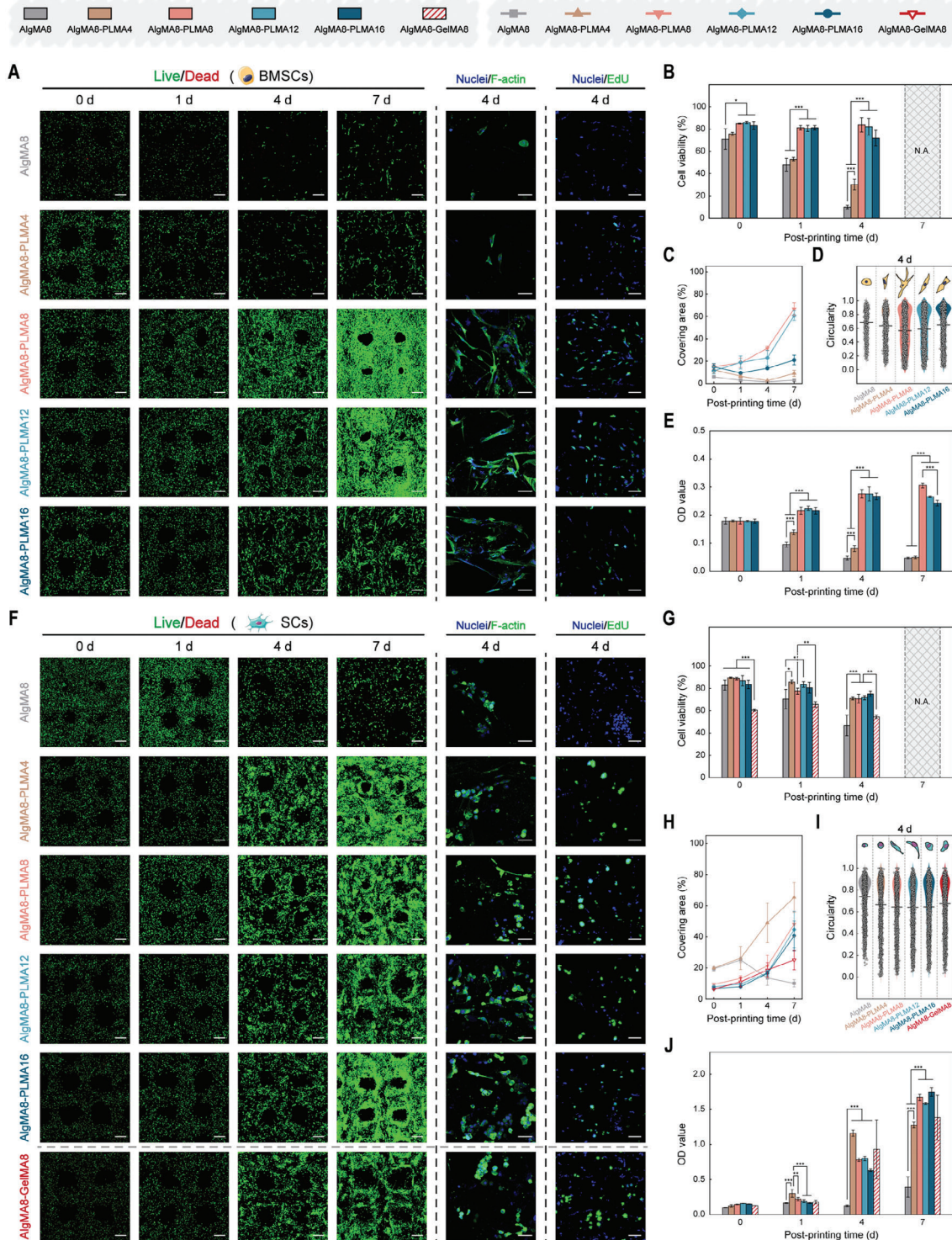


Figure 6. The cell behavior regulation of AlgMA/PLMA bioinks. A) and F) Live/dead fluorescent images of human BMSCs (hBMSCs) (A-left panel) and rat SCs (RSCs) (F-left panel) within AlgMA/PLMA scaffolds at defined time-point. (green: live, red: dead). Scale bar, 400 μ m; Cell morphologies of hBMSCs (A-middle panel) and RSCs (F-middle panel) within AlgMA/PLMA scaffolds after 4 days of culture. (green: F-actin; blue: nuclei). Scale bar, 50 μ m; Cell proliferation of hBMSCs (A-right panel) and RSCs (F-right panel) within AlgMA/PLMA scaffolds on day 4. (green: EduU; blue: nuclei). Scale bar, 50 μ m. B) and G) Cell viability of hBMSCs (B) and RSCs (G) within AlgMA/PLMA scaffolds. The values were obtained by counting the live and dead cells in images from (A-left panel) and (F-left panel) via ImageJ. Because of cell overlap, the scaffolds on day 7 can't be analyzed, thus marked with N.A. C) and H) Cell covering areas of hBMSCs (C) and RSCs (H) on the AlgMA/PLMA scaffolds. D) and I) Circularity of hBMSCs (D) and RSCs (I) within AlgMA/PLMA scaffolds on day 4. E) and J) Cell proliferation (cck-8 quantification) of hBMSCs (E) and RSCs (J) within AlgMA/PLMA scaffolds during 7 days of culture. AlgMA8-GelMA8 containing RSCs (F-J) was involved as a classic control to compare the biofunctions of PLMA and GelMA. ($n = 3$, * $p < 0.05$, ** $p < 0.01$, *** $p < 0.001$).

culture, respectively. SCs in the AlgMA scaffold were spherical and clustered, which were more obvious at day 7 (Figure S12C, Supporting Information); PLMA promoted the elongation of cells, whereas, the pseudopodia shortened with PLMA content increased from 8% to 16% (w/v) (Figure 6I). Gu et al. studied the SCs behaviors on polyacrylamide gel substrates with varying stiffness, and found SCs on the medium-stiff gel (elastic modulus 7.45 kPa) had the largest spreading than that on 4.42, 9.10 kPa, and 12.04 kPa gels.^[33] Thus, similar to AlgMA/PLMA-BMSC, the hydrogel stiffness, at least partially, contributed to the RCs spreading differences. Regarding the AlgMA8-GelMA8-SC, the cells had less spreading as well, similar to AlgMA8-PLMA4-SC. The SCs tended to be spherical and clustered within AlgMA/GelMA hydrogel, despite GelMA content changing from 2.5% to 10% (w/v).^[34]

Collectively, the introduction of the cationic crosslinker ϵ -PLMA can greatly improve the survival and spreading of cells in the AlgMA/PLMA scaffolds. This phenomenon from cationic pre-crosslinker also aligns with our and other groups' previous studies.^[14,35] In the former work, we found that the ϵ -PL modified Alg could promote protein absorption and cell spreading, however, due to the EDC-NHS crosslinking, the material could not serve as cell-printing ink.^[14] Indeed, the electrostatic force is crucial in cell attachment, leading to cell bonding and initiating the focal adhesion with biomaterials. Besides, during cell-material interaction, protein is an important intermediary within this process. In the physiological condition, proteins are usually negatively charged, preferring to accumulate on a positively charged surface.^[36] It is worth noting that, within the AlgMA/PLMA system, adjusting PLMA content not only changes the hydrogel charges, but also the hydrophilicity, the crosslinking density, and stiffness. Therefore, we believe the different cell responses observed in this study are results of a comprehensive regulation, with one or two factors playing the key role.

Harnessing the cell modulation capacity, during organ in vitro manufacture, it is reasonable to deposit inks with different PLMA for spatiotemporally regulating the tissue/organ regeneration process. In comparison with the addition of recombinant nerve growth factor or other biological cues, the ink itself mediated regulation could be more controllable, precise, and cost-effective. For further improvement, replacing the covalent crosslink with dynamic crosslink, e.g., host-guest interaction, could benefit cell migration and proliferation. With the help of fast reversible physical pre-crosslinker, the ink shear-thinning and self-healing behavior will be further improved, giving a more comprehensive range of adjustments of the ink solid content^[37] to meet cell-specific microenvironment requirements.^[38] Additionally, considering the broad application of bioprinting, more cell types, e.g., endothelial cells for vascularization, myocardial cells for myogenesis, and induced pluripotent stem cells for *de novo* tissue/organ development, should be enrolled in the coming study. As well as comprehensive long-term cell functional assessment to further identify the optimal application scenarios of AlgMA/PLMA bioink.

3. Conclusion

In summary, several cyto-benefit pre-/post-crosslinkers with different molecular weights were introduced into Alg-based bioink

to realize high printability before crosslinking of printed structure, and also high biocompatibility and crosslinking stability after crosslinking, respectively. Compared with other Alg-based bioinks, ϵ -PLMA, as a small-molecule pre-crosslinker, can be well mixed in a relatively shorter time than single- and large-molecule pre-crosslinkers. Additionally, this cell-benefit ink preparation process gave a possibility of large-volume ink production, making the foundation of large-scale manufacturing. Furthermore, electrostatic force pre-crosslinking and photo-induced post-crosslinking can co-reinforce the printability and stability of bio-scaffolds. More importantly, the small-molecule polyelectrolyte used here could neutralize the negatively charged environment in Alg, and cells in the bio-scaffolds exhibited improved proliferation and spreading. Notably, the charge environment was totally controlled by the dosage of the pre-crosslinker. We believe this study brings a new view on revitalizing classic Alg-based hydrogels via applying small-molecule cationic crosslinker, paving the way for cell-printing bioinks.

4. Experimental Section

Synthesis of AlgMA: First, Alg (Sigma–Aldrich, Inc.) solution (1% (W/V), 100 ml) was prepared with phosphate buffered saline (PBS). Then, under the condition of ice bath, the MA solution (30 ml) was dropped into the Alg solution drop by drop and reacted in dark for 48 h. During the reaction process, the pH value was controlled between 7–8 by continuously adding NaOH solution dropwise. When the reaction was complete, absolute ethanol was added to the reaction solution to precipitate AlgMA. After this, AlgMA was collected by centrifugation, and then redissolved with double distilled water (ddH₂O). Then, the AlgMA solution was put into a dialysis bag (7 kDa; Solarbio, Inc.) for 72 h dialysis. Then, the AlgMA solution was placed in an ultra-low temperature refrigerator 12 h for freezing. Finally, solid AlgMA was lyophilized for 72 h to obtain the sample AlgMA. AlgMA was characterized by Fourier transform infrared spectrometer (FTIR) and ¹H and ¹³C nuclear magnetic resonance (¹H NMR and ¹³C NMR). Detailed methods and results can be found in Supporting Information.

Synthesis of ϵ -PLMA: First, ϵ -PL (Macklin, Inc.) solution (5%, 100 ml) was prepared with PBS. Then, under the condition of ice bath, the methacrylic anhydride (MA, Sigma, Inc.) solution (1.5 ml) was added into the ϵ -PL solution drop by drop and reacted in dark for 6 h. During the reaction process, the pH value was 7–8. After the reaction, the precipitate in the reaction solution was removed by centrifugation; the reaction solution was placed in a dialysis bag (300 Da; Solarbio, Inc.) for 72 h dialysis. Finally, the dialysis solution was placed in an ultra-low temperature refrigerator for 12 h, and then lyophilized for 72 h to obtain the sample— ϵ -PLMA. ϵ -PLMA was characterized by Fourier transform infrared spectrometer (FTIR) and ¹H nuclear magnetic resonance (¹H NMR). Detailed methods and results can be found in Supporting Information.

Characterization of AlgMA/PLMA Bioinks: Different solid content ϵ -PLMA sample and AlgMA sample were dissolved in the MEM culture solution containing 0.1% LAP photo-initiator (refer to Table S1, Supporting Information). AlgMA/PLMA series bioinks were performed with the following tests to evaluate their properties: water contact angle (WCA), water absorption (WA) test, degradation test, kelvin probe force microscopy (KPFM), mechanical compression test, and rheological test. Detailed methods can be found in Supporting Information.

Preparation and Printing of Bioink: hBMSCs or RSCs suspensions were added and mixed well to get AlgMA/PLMA bioink. The prepared AlgMA/PLMA bioinks were filled into a plastic transparent printing syringe, and then the designed cube 3D scaffold model was imported into an extrusion 3D printer. Driven by a pneumatic pump, inks were extruded into the Petri dish through a 40[#] (400 μ m) tapered nozzle. The scaffold lines of

adjacent layers were printed at 90° rotation, and the lines were deposited layer by layer to form a cell scaffold. Then, a UV flashlight was used to irradiate the printed cell scaffolds to make them UV-crosslinked and form stable structures, and then the AlgMA/PLMA series cell scaffolds can be obtained. Finally, scaffolds were placed in the cell culture well plate, and an appropriate amount of MEM culture solution was added, so that the MEM culture solution just covered the scaffold. Then, they were placed in the cell culture incubator for 7 days. The culture temperature was 37 °C, the CO₂ concentration was 5%, and the MEM culture medium was replaced every 2 d.

Evaluation of Printability of Alg-Based Inks: A high-definition camera was used to characterize the shape and structure of the prepared four kinds of Alg-based scaffolds.

1) **Mesh size (MS) Analysis:** Before crosslinking of these four kinds of printed scaffolds, scaffolds were observed and recorded by a camera on 0 s (printed), 10 s, and 5 min. The MS was calculated on software ImageJ by labelling the area of 36 meshes in the middle of a scaffold.

2) **Printability (Pr.) Analysis:** When the bioink was in an ideal gelation condition, the extruded filament would demonstrate a clear morphology with smooth surface and constant width, which would result into regular square meshes in the fabricated constructs.^[20] When the bioink was in an under-gelation condition, the extruded filament would demonstrate a more liquid-like state, and the upper layer would fuse with the lower layer, thus creating approximately circular meshes.^[20]

Circularity (C) of an enclosed area was defined as the following Equation 1:

$$C = \frac{4\pi A}{L^2} \quad (1)$$

And according to Ouyang et al., Pr. was calculated as Equation 2:

$$Pr = \frac{\pi}{4} \times \frac{1}{C} \quad (2)$$

where L means perimeter and A means area. Circles have the highest circularity (C = 1). The closer the C value was to 1, the closer the shape is to a circle.

3) **Shape Maintenance (SM) Analysis:** The SM of 10 s was calculated as the MS of 10 s was divided by the MS of 0s. The SM of 10 s was calculated as the MS of 5 min was divided by the MS of 0 s. The SM of the sample was calculated according to Equation 3 (n is the time period after printing):

$$SM_n = \frac{MS_n}{MS_0} \quad (3)$$

where n = 10 s, 5 min, representing the time point of test.

4) **Printing Stability (PS) Analysis:** The PS was calculated from at least three scaffolds with 36 meshes from each of them. In a single scaffold, the mesh size should be uniform, if the ink had an excellent printing stability. If not, the size of meshes in single scaffold may have a large diversity. To calculate the PS, the average of the mesh size (A_{MS}) and the standard deviation of the average mesh size (S_{MS}) should be obtained. A_{MS} can be calculated as Equation 4:

$$A_{MS} = \frac{\sum_{i=1}^n MS_i}{n} \quad (4)$$

And S_{MS} can be calculated as Equation 5:

$$S_{MS} = \sqrt{\frac{\sum_{i=1}^n (MS_i - A_{MS})^2}{n - 1}} \quad (5)$$

where n = 1, 2, 3, …, n, representing the number of meshes.

And the PS was defined as the proportion of S_{MS} to A_{MS}, which can be calculated as Equation 6:

$$PS = \frac{S_{MS}}{A_{MS}} \quad (6)$$

Evaluation of Crosslinking Stability of Alg-based Inks: Same as the part 4.7.2., the scaffolds were crosslinked immediately after they were printed. They were put into 6-well plates on a shaker at 37 °C (60 r min⁻¹, soaked for 28d). A high-definition camera was used to characterize the shape and structure of the prepared four kinds of Alg-based scaffolds on 0 d (crosslinked), 1 d, 7 d, 14 d, and 28 d. To calculate the crosslinking stability (CS), the scaffold size (SS) should be obtained. The CS of 7 d was calculated as the SS of 7 d is divided by the SS of 0 s (SS₀). The changing of scaffold size (CSS) can be calculated as Equation 7:

$$CSS_n = \frac{SS_n}{SS_0} \quad (7)$$

And CS can be calculated as Equation 8:

$$CS_n = \ln CSS_n \quad (8)$$

where n = 1, 7, 14, 28, representing the time point of test.

The best CS was 0 and the swell and shrink of scaffolds reflects on a positive and negative number, respectively.

Live/Dead Test: Bioinks with 2 × 10⁶ ml⁻¹ hBMSCs or RSCs were prepared, respectively. Throughout the printing process, the pressure was constantly held at 45 kPa, while the printing speed was adjusted to match different formulations. The optimized printing speeds were provided in Table S2 (Supporting Information). Immediately after the printing was completed, the cell culture well plate on which the AlgMA/PLMA cell scaffolds were cultivated was removed, the MEM culture solution in the well plate was discarded, and the scaffold was soaked with PBS solution 3 times, each time for 5 minutes (minute, min). Then, at ambient temperature, 2 mL of prepared FDA-PI dual dye was added to each well of the well plate, and scaffolds were submerged by the dye, and stained in the dark for 20 min. After staining, scaffolds were removed and rinsed with PBS solution to remove excess dye. Finally, the AlgMA/PLMA series cell scaffolds were placed in glass-bottom dishes, observed through a confocal laser scanning microscope (ECLIPSE Ti2; Nikon, Inc.) and photographed for record.

To explore the effect of extrusion pressure on the survival of cells in the ink during printing, the specific operation steps were as follows: printing extrusion pressures were set 60, 80, and 100 kPa to print AlgMA8-PLMA8 ink to obtain cell scaffolds; and 4 h after printing, the cell scaffolds were tested for cell viability staining.

Nuclei and Actin Staining: The staining was performed according to the manufacturers' instructions (Hoechst 33342, Beyotime; anti-Actin antibody, Proteintech; Alexa Fluor 488 conjugated goat anti-mouse IgG, Beyotime). Briefly, at the designed timepoint, the cultured AlgMA/PLMA scaffolds were fixed with 4% paraformaldehyde (PFA, Macklin) for 15 min at room temperature (RT), then permeabilized with 0.2% Triton X-100 (Sigma) for 10 min at RT, followed by 1 h blocking with 1% BSA-PBST (PBS containing 0.2% Tween 20, Beyotime); Subsequently, the scaffolds were overnight incubated with anti-actin antibody (1:500 dilution) at 4 °C under gentle agitation; After washing in PBS three times, 5 min each, the Alexa Fluor 488 conjugated goat anti-mouse IgG antibody (1:500 dilution) was added, and incubated at RT for 2 h; Last, the nuclei were counterstained with Hoechst 33 342 (5 μg ml⁻¹) for 15 min at RT. The samples were placed in glass-bottom dishes, and photographed by a confocal laser scanning microscope (ECLIPSE Ti2; Nikon, Inc.).

Nuclei and EdU Staining: To label the proliferated cells, the EdU imaging kit (APEX BIO, China) was applied. At the designed time-point, the EdU solution was added to the culture media with a final EdU concentration at 20 μM; After 12 h incubation, the scaffolds were fixed with 4% PFA for 15 min at RT, followed by washing with 3% BSA-PBS for 3 times, 5 min each; Then, using 0.2% Triton X-100 to permeabilize the cells within

the scaffolds for 10 min at RT, followed by washing with 3% BSA-PBS for twice, 5 min each; Incubate the scaffolds in click reaction mixture for 30 min in the dark at RT, followed by washing with 3% BSA-PBS for 3 times, 5 min each; In the end, the nuclei were counterstained with Hoechst 33 342 (5 µg ml⁻¹) for 15 min at RT. The samples were placed in glass-bottom dishes, and photographed by a confocal laser scanning microscope (ECLIPSE Ti2; Nikon, Inc.).

Statistical Analysis: All data were expressed as mean ± SD, and the data were visualized using Origin Pro software; CCK-8 data and mechanical compression modulus data were subjected to one-way analysis of variance using Tukey's post hoc test, and the P values for significant differences were **p* < 0.05, ***p* < 0.01, ****p* < 0.001.

Supporting Information

Supporting Information is available from the Wiley Online Library or from the author.

Acknowledgements

C.G. and L.T. contributed equally to this work. The authors gratefully acknowledge the support for this work from the National Key Research and Development Program (grant nos. 2022YFA1207502 and 2018YFA0703100); the National Natural Science Foundation of China (grant nos. 32122046, 82072082, 32000959, 32101102, and 32201097); the Guangdong Natural Science Foundation (grant no. 2020A1515111190); the Shenzhen Fundamental Research Foundation (grant nos. JCYJ20200109114006014, JCYJ20210324115814040, JCYJ20210324113001005, and JCYJ20220531100602004); National Key Clinical Specialty Construction Project (no. SZXK015) and Guangdong High-level Clinical Key Specialties (no. SZGSP001); Shenzhen Science and Technology Program (no. JSGGKQTD20210831174330015).

Conflict of Interest

The authors declare no conflict of interest.

Data availability Statement

The data that support the findings of this study are available from the corresponding author upon reasonable request.

Keywords

alginate-based bioinks, extrusion bioprinting, printability, shape maintenance, ε-polylysine

Received: August 29, 2023
Revised: November 7, 2023
Published online:

- [1] a) R. L. Truby, J. A. Lewis, *Nature* **2016**, *540*, 371; b) M. A. Skylar-Scott, J. Mueller, C. W. Visser, J. A. Lewis, *Nature* **2019**, *575*, 330; c) Q. Dasgupta, L. D. Black, *Science* **2019**, *365*, 446; d) A. C. Daly, M. E. Prendergast, A. J. Hughes, J. A. Burdick, *Cell* **2021**, *184*, 18; e) P. Wang, H. Rui, C. Gao, C. Wen, H. Pan, W. Liu, C. Ruan, W. W. Lu, *The Innov. Life* **2023**, *1*, 100019.
[2] N. E. Fedorovich, J. R. De Wijn, A. J. Verbout, J. Alblas, W. J. A. Dhert, *Tissue Eng., Part A* **2008**, *14*, 127.

- [3] O. Jeon, Y. B. Lee, T. J. Hinton, A. W. Feinberg, E. Alsberg, *Mater. Today Chem.* **2019**, *12*, 61.
[4] Y. Zhang, Y. Yu, A. Akkouch, A. Dababneh, F. Dolati, I. T. Ozbolat, *Biomater. Sci.* **2015**, *3*, 134.
[5] A. Schulz, M. M. Gepp, F. Stracke, H. Von Briesen, J. C. Neubauer, H. Zimmermann, *J. Biomed. Mater. Res. A* **2019**, *107*, 114.
[6] J. A. Rowley, G. Madlambayan, D. J. Mooney, *Biomaterials* **1999**, *20*, 45.
[7] a) Q. Pi, S. Maharjan, X. Yan, X. Liu, B. Singh, A. M. Van Genderen, F. Robledo-Padilla, R. Parra-Saldivar, N. Hu, W. Jia, C. Xu, J. Kang, S. Hassan, H. Cheng, X. Hou, A. Khademhosseini, Y. S. Zhang, *Adv. Mater.* **2018**, *30*, 1706913; b) G.-L. Ying, N. Jiang, S. Maharjan, Y.-X. Yin, R.-R. Chai, X. Cao, J.-Z. Yang, A. K. Miri, S. Hassan, Y. S. Zhang, *Adv. Mater.* **2018**, *30*, 1805460; c) L. Ouyang, J. P. K. Armstrong, Y. Lin, J. P. Wojciechowski, C. Lee-Reeves, D. Hachim, K. Zhou, J. A. Burdick, M. M. Stevens, *Sci. Adv.* **2020**, *6*, eabc5529; d) A. P. Dhand, J. H. Galarraga, J. A. Burdick, *Trends Biotechnol.* **2021**, *39*, 519.
[8] U. Hersel, C. Dahmen, H. Kessler, *Biomaterials* **2003**, *24*, 4385.
[9] J. P. Gong, Y. Katsuyama, T. Kurokawa, Y. Osada, *Adv. Mater.* **2003**, *15*, 1155.
[10] W. Jia, P. S. Gungor-Ozkerim, Y. S. Zhang, K. Yue, K. Zhu, W. Liu, Q. Pi, B. Byambaa, M. R. Dokmeci, S. R. Shin, A. Khademhosseini, *Biomaterials* **2016**, *106*, 58.
[11] G. Kretzmer, K. Schögerl, *Appl. Microbiol. Biotechnol.* **1991**, *34*, 613.
[12] H. Nulwala, A. Mirjafari, X. Zhou, *Eur. Polym. J.* **2018**, *108*, 390.
[13] H. Wang, M. B. Hansen, D. W. Lowik, J. C. van Hest, Y. Li, J. A. Jansen, S. C. Leeuwenburgh, *Adv. Mater.* **2011**, *23*, H119.
[14] Z. Lin, M. Wu, H. He, Q. Liang, C. Hu, Z. Zeng, D. Cheng, G. Wang, D. Chen, H. Pan, C. Ruan, *Adv. Funct. Mater.* **2019**, *29*, 1808439.
[15] K. S. Lim, J. H. Galarraga, X. Cui, G. C. J. Lindberg, J. A. Burdick, T. B. F. Woodfield, *Chem. Rev.* **2020**, *120*, 10662.
[16] a) O. Jeon, K. H. Bouhadir, J. M. Mansour, E. Alsberg, *Biomaterials* **2009**, *30*, 2724; b) X. Wang, J. Qi, W. Zhang, Y. Pu, R. Yang, P. Wang, S. Liu, X. Tan, B. Chi, *Int. J. Biol. Macromol.* **2021**, *187*, 91.
[17] A. G. Tabriz, M. A. Hermida, N. R. Leslie, W. Shu, *Biofabrication* **2015**, *7*, 045012.
[18] L. Ouyang, *Trends Biotechnol.* **2022**, *40*, 891.
[19] a) A. Schwab, R. Levato, M. D'este, S. Piluso, D. Eglin, J. Malda, *Chem. Rev.* **2020**, *120*, 11028; b) K. Song, A. M. Compaan, W. Chai, Y. Huang, *ACS Appl. Mater. Interfaces* **2020**, *12*, 22453.
[20] L. Ouyang, R. Yao, Y. Zhao, W. Sun, *Biofabrication* **2016**, *8*, 035020.
[21] J. Gong, C. C. L. Schuurmans, A. M. V. Genderen, X. Cao, W. Li, F. Cheng, J. J. He, A. López, V. Huerta, J. Manríquez, R. Li, H. Li, C. Delavaux, S. Sebastian, P. E. Capendale, H. Wang, J. Xie, M. Yu, R. Masereeuw, T. Vermonden, Y. S. Zhang, *Nat. Commun.* **2020**, *11*, 1267.
[22] L. Xu, W. Chen, A. Mulchandani, Y. Yan, *Angew. Chem. Int. Ed. Engl.* **2005**, *44*, 6009.
[23] a) Y. Arima, H. Iwata, *Biomaterials* **2007**, *28*, 3074; b) M. Mohammadalipour, M. Asadolahi, Z. Mohammadalipour, T. Behzad, S. Karbasi, *Int. J. Biol. Macromol.* **2023**, *230*, 123167.
[24] Y. Liu, L. Peng, L. Li, C. Huang, K. Shi, X. Meng, P. Wang, M. Wu, L. Li, H. Cao, K. Wu, Q. Zeng, H. Pan, W. W. Lu, L. Qin, C. Ruan, X. Wang, *Biomaterials* **2021**, *279*, 121216.
[25] a) R. Schwartz, M. Malpica, G. L. Thompson, A. K. Miri, *J. Mech. Behav. Biomed. Mater.* **2020**, *103*, 103524; b) T. Gregory, P. Benhal, A. Scutte, D. Quashie, K. Harrison, C. Cargill, S. Grandison, M. J. Savitsky, S. Ramakrishnan, J. Ali, *J. Mech. Behav. Biomed. Mater.* **2022**, *136*, 105474.
[26] A. Blaesser, D. F. Duarte Campos, U. Puster, W. Richtering, M. M. Stevens, H. Fischer, *Adv. Healthc. Mater.* **2016**, *5*, 326.
[27] W. Liu, M. A. Heinrich, Y. Zhou, A. Akpek, N. Hu, X. Liu, X. Guan, Z. Zhong, X. Jin, A. Khademhosseini, Y. S. Zhang, *Adv. Healthc. Mater.* **2017**, *6*, 1601451.

- [28] C. M. Murphy, M. G. Haugh, F. J. O'Brien, *Biomaterials* **2010**, *31*, 461.
- [29] a) R. Mcbeath, D. M. Pirone, C. M. Nelson, K. Bhadriraju, C. S. Chen, *Dev. Cell* **2004**, *6*, 483; b) Y. Yang, X. Wang, Y. Wang, X. Hu, N. Kawazoe, Y. Yang, G. Chen, *Sci. Rep.* **2019**, *9*, 6891; c) P. A. Janmey, B. Hinz, C. A. McCulloch, *Physiology* **2021**, *36*, 382.
- [30] M. Sun, G. Chi, P. Li, S. Lv, J. Xu, Z. Xu, Y. Xia, Y. Tan, J. Xu, L. Li, Y. Li, *Int. J. Med. Sci.* **2018**, *15*, 257.
- [31] Y. Wang, Y. Ji, Y. Zhao, Y. Kong, M. Gao, Q. Feng, Y. Wu, Y. Yang, *J. Biomater. Appl.* **2016**, *30*, 1494.
- [32] M. H. Lee, D. A. Brass, R. Morris, R. J. Composto, P. Ducheyne, *Biomaterials* **2005**, *26*, 1721.
- [33] Y. Gu, Y. Ji, Y. Zhao, Y. Liu, F. Ding, X. Gu, Y. Yang, *Biomaterials* **2012**, *33*, 6672.
- [34] Z. Wu, S. Xie, Y. Kang, X. Shan, Q. Li, Z. Cai, *Mater. Sci. Eng. C Mater. Biol. Appl.* **2021**, *129*, 112393.
- [35] H. Liu, Y. Wang, Y. Yu, W. Chen, L. Jiang, J. Qin, *J. Biomed. Mater. Res. B Appl. Biomater.* **2019**, *107*, 2527.
- [36] R. A. Hartvig, M. Van De Weert, J. Østergaard, L. Jorgensen, H. Jensen, *Langmuir* **2011**, *27*, 2634.
- [37] a) C. B. Highley, C. B. Rodell, J. A. Burdick, *Adv. Mater.* **2015**, *27*, 5075; b) C. B. Rodell, N. N. Dusaj, C. B. Highley, J. A. Burdick, *Adv. Mater.* **2016**, *28*, 8419.
- [38] a) C. F. Guimarães, L. Gasperini, A. P. Marques, R. L. Reis, *Nat. Rev. Mater.* **2020**, *5*, 351; b) Y. Liu, Q. Hu, W. Dong, S. Liu, H. Zhang, Y. Gu, *Macromol. Biosci.* **2022**, *22*, e2100413; c) S. Naeimipour, F. Rasti Boroojeni, R. Selegård, D. Aili, *Chem. Mater.* **2022**, *34*, 9536; d) S. Murab, A. Gupta, M. K. Włodarczyk-Biegun, A. Kumar, P. Van Rijn, P. Whitlock, S. S. Han, G. Agrawal, *Carbohydr. Polym.* **2022**, *296*, 119964.